Robust characterisation of forest structure from airborne laser scanning-A systematic assessment and sample workflow for ecologists

Fabian Jörg Fischer, Toby Jackson, Grégoire Vincent, Tommaso Jucker

RESEARCH ARTICLE

Methods in Ecology and Evolution | BRITISH ECOLOGICAL SOCIETY

Robust characterisation of forest structure from airborne laser scanning—A systematic assessment and sample workflow for ecologists

Fabian Jörg Fischer[1] | Toby Jackson[1,2] | Grégoire Vincent[3] | Tommaso Jucker[1]

[1]School of Biological Sciences, University of Bristol, Bristol, UK

[2]Plant Sciences and Conservation Research Institute, University of Cambridge, Cambridge, UK

[3]AMAP, University of Montpellier, CIRAD, CNRS, INRAE, IRD, Montpellier, France

Correspondence
Fabian Jörg Fischer
Email: f.fischer@bristol.ac.uk

Abstract

1. Forests display tremendous structural diversity, shaping carbon cycling, microclimates and terrestrial habitats. An important tool for forest structure assessments are canopy height models (CHMs): high resolution maps of canopy height obtained using airborne laser scanning (ALS). CHMs are widely used for monitoring canopy dynamics, mapping forest biomass and calibrating satellite products, but surprisingly little is known about how differences between CHM algorithms impact ecological analyses.

2. Here, we used high-quality ALS data from nine sites in Australia, ranging from semi-arid shrublands to 90-m tall Mountain Ash canopies, to comprehensively assess CHM algorithms. This included testing their sensitivity to point cloud degradation and quantifying the propagation of errors to derived metrics of canopy structure.

3. We found that CHM algorithms varied widely both in their height predictions (differences up to 10 m, or 60% of canopy height) and in their sensitivity to point cloud characteristics (biases of up to 5 m, or 40% of canopy height). Impacts of point cloud properties on CHM-derived metrics varied, from robust inference for height percentiles, to considerable errors in above-ground biomass estimates ($\sim$50 Mg ha^{-1}, or 10% of total) and high volatility in metrics that quantify spatial associations in canopies (e.g. gaps). However, we also found that two CHM algorithms—a variation on a 'spikefree' algorithm that adapts to local pulse densities and a simple Delaunay triangulation of first returns—allowed for robust canopy characterisation and should thus create a secure foundation for ecological comparisons in space and time.

4. We show that CHM choice has a strong impact on forest structural characterisation that has previously been largely overlooked. To address this, we provide a sample workflow to create robust CHMs and best-practice guidelines to minimise biases and uncertainty in downstream analyses. In doing so, our study paves the

way for more rigorous large-scale assessments of forest structure and dynamics from airborne laser scanning.

KEYWORDS
airborne laser scanning, canopy gaps, canopy height model, forest structure, lidar, pitfree, spikefree, structural complexity

1 | INTRODUCTION

Forests across the globe display tremendous structural diversity, ranging from open woodlands to tall, dense, multi-layered tropical forests. Quantifying structural differences across and within forest ecosystems is vital, as they shape climate at both small (De Frenne et al., 2021) and large scales (Alkama & Cescatti, 2016), are tightly coupled to carbon fluxes (Fischer et al., 2019) and resource provision (Felipe-Lucia et al., 2018), influence the resilience of forests to disturbance (Koontz et al., 2020) and create habitats for forest-dwelling organisms (Gouveia et al., 2014).

For a long time, the main challenge to quantifying the vertical and horizontal structure of forest canopies was data acquisition. It involved the painstaking delineation of canopy gaps from the ground (Meer & Bongers, 1996) or the manual measurements of tree crowns to generate canopy profile diagrams (Baker & Wilson, 2000). The advent of remote sensing has radically changed this, with ever-increasing opportunities to quantify forest structural complexity (Atkins et al., 2018; Ehbrecht et al., 2021; Fischer & Jucker, 2024). In particular, airborne laser scanning (ALS) has emerged as a key technology in this field, allowing researchers to probe forest canopies from above using high-frequency laser scanners mounted on airplanes, helicopters or even drones. Whenever a laser pulse emitted by the scanner hits an obstacle—a leaf, a branch or the ground—the reflected energy spike can be converted into a geolocated point, capturing the forest as a 3D 'point cloud'. The unique value of these ALS-derived point clouds is the ability to characterise forest structure and topography in high detail (e.g. 1-m^2 resolution), while also covering areas large enough (e.g. 10s of km^2) to map landscape patterns (Lines et al., 2022). With large-scale coverage available in many countries, ALS is now a tool ready for global ecological analysis (Jucker, 2022).

A particularly useful feature of ALS point clouds is that they can be used to generate high-resolution maps of canopy height, known as canopy height models (CHMs). CHMs are 2.5 dimensional representations of canopies that primarily rely on top-canopy returns from ALS pulses. They sacrifice some of the 3D information contained in point clouds, but in return gain robustness to differences in instrumentation, acquisition platform and flight parameters (Asner, Mascaro, et al., 2013; Mielcarek et al., 2018; Zhang et al., 2024). They are also smaller in data volume than point clouds, easier to manipulate and can be accompanied by rasterised metadata, which makes them highly accessible to non-expert users. ALS-derived CHMs are already widely used for forest carbon mapping (Asner, Mascaro,

et al., 2013; Coomes et al., 2017; Labriere et al., 2018), tree delineation (Aubry-Kientz et al., 2019; Kaartinen et al., 2012), modelling of forest attributes (Bottalico et al., 2017; Næsset, 2002), studies of canopy dynamics and gaps (Asner, Kellner, et al., 2013; Dalagnol et al., 2021; Goodbody et al., 2020; Huertas et al., 2022), the calibration of forest models (Fischer et al., 2020) and habitat assessments (Davies & Asner, 2014; Zellweger et al., 2013). CHMs are also expected to play an increasingly important role in the calibration of global satellite products (e.g. through initiatives like GEO-TREES, https://geo-trees.org). Moreover, growing access to multi-temporal ALS surveys (e.g. through networks like NEON, https://www.neonscience.org) make CHMs a simple, yet powerful tool to monitor fine-scale canopy dynamics at increasingly large scales (Jucker, 2022).

However, to leverage the full potential of CHMs for ecological research, we first need to better understand how sensitive they are to the properties of the point clouds from which they are derived, so that we can develop standardised pipelines for generating them (Moudrý et al., 2023). While considerable effort has gone into optimising ALS-derived terrain models (Andrade et al., 2018; Chen et al., 2017) and point cloud-derived metrics (Almeida et al., 2019; Magnussen et al., 2010; Næsset, 2009; Pearse et al., 2019; Riofrío et al., 2022; Roussel et al., 2018; Vincent et al., 2023; Wilkes et al., 2015), there is surprisingly little guidance for ecologists on how to generate robust CHMs that are comparable across instruments and sampling designs. For example, the most frequent approach to obtaining CHMs is to rasterise the highest point at a target resolution and then subtract the resulting surface model from a digital terrain model. This is accurate when the density of emitted pulses (or their returns) is high (e.g. ≥20 pulses m^{-2}), but will underestimate canopy height at low pulse densities, as laser shots miss branches and leaves or fail to produce ground returns (LaRue et al., 2022; Leitold et al., 2015; Roussel et al., 2017). Pulse density is likely the strongest determinant of CHM quality but bias can also result from variations in laser energy, scan angles and footprint size (Keränen et al., 2016; Næsset, 2009; Roussel et al., 2017, 2018). Several algorithms have been developed to improve CHM robustness (e.g. Khosravipour et al., 2014, 2016), some of which are available in open-source software such as the lidR R package (Roussel et al., 2020). However, assessments of multiple CHM algorithms have so far been limited to single acquisitions or reference height points (Mielcarek et al., 2018; Quan et al., 2021).

Here we use ALS data from nine sites in Australia that cover a wide range of ecosystems—from open acacia woodlands to dense rain forests and 90-m tall Mountain Ash stands—and assess the robustness

TABLE 1 Forest and scan characteristics across the nine TERN SuperSites.

Site	Lon	Lat	Forest type	Elevation (m a.s.l.)	Maximum canopy height (m)	Canopy cover (%)	Pulse density (m⁻²)	Ratio 2nd/1st returns	Scan date
Alice Mulga	133.25	−22.28	Semi-arid acacia woodland	600	8.0	65	24.9	0.51	06/2015
Chowilla	140.59	−34.00	Semi-arid mallee shrubland	50	10.1	43	20.6	0.33	02/2012
Credo	120.66	−30.19	Semi-arid temperate woodland	450	22.3	29	21.5	0.24	05/2012
Litchfield	131.79	−13.18	Tropical savanna	220	25.6	49	20.8	0.31	06/2013
Rushworth Forest	144.96	−36.75	Dry sclerophyll forest	200	25.6	71	19.1	0.54	04/2012
Robson Creek	145.62	−17.11	Seasonal tropical rainforest	870	53.6	100	31.0	0.45	09/2012
Zigzag Creek	148.34	−37.47	Dry/wet sclerophyll forests	280	55.0	92	19.2	0.34	04/2012
Warra	146.66	−43.10	Wet sclerophyll forest	250	75.1	97	20.2	0.57	01/2015
Watts Creek	145.69	−37.69	Wet sclerophyll forest	990	87.0	97	19.0	0.66	04/2012

Note: Coordinates, elevation and canopy properties are derived from digital terrain models (DTMs) and canopy height models (CHMs) calculated from the original scans via the 'locally adaptive spikefree' method (CHM$_{lspikefree}$; see Section 2.2 for details). Maximum canopy height was calculated as the 99th percentile of the CHM, while canopy cover is defined as the proportion of CHM pixels taller than 2 m above-ground. Sites are ordered by maximum canopy height.

of six CHM algorithms, including two newly developed variations. By systematically manipulating laser point clouds, we test: (1) What are the main sources of uncertainty and bias in CHMs? (2) Which algorithms are most robust to differences in acquisition parameters and point cloud degradation? And (3) how do errors in CHM construction propagate to canopy structural attributes such as canopy gaps, canopy heterogeneity and above-ground biomass estimates?

We summarise our results into 16 best-practice guidelines for ecologists and provide a versatile pipeline for producing robust CHMs in R. In doing so, we aim to raise awareness around some of the main challenges of creating and comparing CHMs, while also facilitating the use of ALS data for large-scale and multi-temporal analyses across ecological disciplines.

2 | MATERIALS AND METHODS

2.1 | ALS data

Airborne laser scanning data were obtained from nine SuperSites belonging to Australia's Terrestrial Ecosystem Research Network (TERN; Karan et al., 2016). These sites provide an ideal testbed for assessing the robustness of CHM algorithms. For one, they range widely in mean annual temperature (8.4–27.3°C), annual precipitation (260–1950 mm) and elevation (50–1000 m a.s.l.), resulting in a considerable variety of canopy structures: maximum heights between 10 and 90 m and 30%–100% canopy cover (Table 1). Moreover, in 2012–15, all sites were scanned over a consistent 5 × 5 km^2 extent with a Riegl Q560 scanner in full-waveform mode (outgoing pulse rate of 240 kHz, wavelength of 1550 nm) and logged on a Riegl DR560 data recorder. Raw waveforms were then discretised via 'Gaussian Estimation' (RiAnalyze 4.1.2). The majority of sites were scanned in 41 parallel flightlines (aligned either N-S or E-W), spaced 125 m apart and with a 45° sweep, comprising 882 laser shots. Exceptions were tall Eucalypt stands in Warra, Tasmania (50 flightlines), and Robson Creek, a dense, high-biomass rain forest in northern Queensland, which was scanned over 2 days (112 flightlines, both N-S and E-W) to capture the site's complex canopy and topography. Nominal flying height was 300 m throughout, resulting in a maximum footprint diameter of 0.15 m and high sampling densities (19–31 pulses m^{-2}).

2.2 | A standardised workflow for generating CHMs from ALS point clouds

2.2.1 | Point cloud processing

We developed a standardised pipeline to convert ALS point clouds into digital terrain models (DTMs) and canopy height models (CHMs). The pipeline is executed from R (R Core Team, 2023) and processes data with a combination of LAStools commands (Isenburg, 2023, called directly from R via 'system()') and custom functions, mostly relying on the lidR, terra and data.table packages (Dowle &

Srinivasan, 2023; Hijmans, 2023; Roussel et al., 2020). The pipeline was developed for the automatic processing of large volumes of data with variable structures and has been extensively tested across scans and sites (Jackson et al., 2024; Rosen et al., 2024). Further details on the pipeline and R packages can be found in the Supplementary Information (S1). The code and a sample workflow are available on Zenodo (http://doi.org/10.5281/zenodo.10878070). For the purposes of this analysis, ALS point clouds were processed in tiles of 500 m, with buffers of 25 m. All processing was carried out in parallel on an Intel® Core™ i9-10980XE CPU with 18 physical cores and 64 GB of RAM.

2.2.2 | CHM algorithms

As part of the processing pipeline, we used six alternative CHM algorithms (see extended descriptions in Table 2). Four are part of common software tools (LAStools, lidR) and run with recommended parameterisations to generate $1\,m^2$ resolution CHMs. We chose a $1\,m^2$ resolution as this is the default for many ALS-based raster products—for example CHMs provided by NEON (https://www.neonscience.org) and OpenTopography (https://opentopography.org)—and a common resolution in forest structure analysis (Dalagnol et al., 2021; Labriere et al., 2018; Silva et al., 2019). The CHM

TABLE 2 Canopy height model (CHM) algorithms.

Algorithm	Abbreviation	Description
First-return TIN	CHM_{tin}	Delaunay triangulation of ALS first returns, as implemented in the *LAStools* blast2dem function. Performed on the non-normalised point cloud to create a $1\,m^2$ resolution DSM. The CHM is derived by subtracting the DTM from the DSM
Highest return raster	$CHM_{highest}$	Gridding of highest returns at $1\,m^2$ resolution using lasgrid, and CHM creation via subtraction of DTM from DSM
Pitfree algorithm	$CHM_{pitfree}$	Pitfree algorithm (Khosravipour et al., 2014), as described in *LAStools* batch procedures (https://github.com/LAStools/LAStools/blob/master/example_batch_scripts, accessed on 7 February 2023). Moves through the normalised point cloud vertically and creates intermediate CHMs that are then combined into a final 'pitfree' CHM at $1\,m^2$ resolution. Carried out with standard parameters, including thinning at half the target resolution ($0.25\,m^2$), 'splatting out' of returns (radius = 0.05 m) and removal of Delaunay triangles in intermediate CHMs with edge lengths larger than three times the target resolution ($3 \times 1\,m = 3\,m$). Intermediate CHMs were computed at 5 m vertical steps. A DSM was obtained by summing DTM and CHM
Spikefree algorithm	$CHM_{spikefree}$	Constrained Delaunay triangulation (Khosravipour et al., 2016). Triangulates points that are nearby both horizontally and vertically and omits non-relevant returns below already triangulated areas. Conceived as update to the pitfree algorithm and implemented on non-normalised point clouds via las2dem. The so-called 'freeze constraint' parameter is set to three times the average pulse spacing, or sqrt(1/pulse density). Note that this is not the original implementation, but a common heuristic described in the *LAStools* documentation (https://rapidlasso.com/2016/02/03/generating-spike-free-digital-surface-models-from-lidar/, accessed on 7 February 2023). Used to create a $1\,m^2$ resolution DSM from non-normalised returns; converted to CHM via DTM subtraction
Spikefree algorithm (thinned point cloud)	$CHM_{tspikefree}$	Same as the spikefree algorithm, but based on a systematically thinned and homogenised point cloud (2 pulses per m^2). Thinning is performed with the lasthin function at $1\,m^2$ resolution, retaining only first returns to increase robustness across instruments. The freeze constraint is set to $3 \times$ sqrt(1/2) m, or ~2.1 m
Spikefree algorithm (locally adaptive)	$CHM_{lspikefree}$	Same as the spikefree algorithm, but using only first returns and a freeze-constraint adapted to local pulse densities. The algorithm first computes local pulse densities across $5 \times 5\,m^2$ patches and divides the scan area into clusters belonging to the same pulse density class. Pulse density classes are defined in steps of 0.5 from 0 to 3 pulses m^{-2}, steps of 1 from 3 to 10 pulses m^{-2}, steps of 2 to from 10 to 20 pulses m^{-2}, step of 5 from 20 to 50 pulses m^{-2}, and steps of 25 from 50 to 100 pulses m^{-2}. Point cloud areas with pulse densities >100 m^{-2} are processed as if their pulse density was 100 m^{-2}. For each cluster belonging to the same pulse density class, we create a buffer zone of $5 \times 5\,m^2$ and compute a DSM with a pulse density adapted freeze constraint. The freeze constraint is determined as: freeze $= m_{freeze} / (\ln(s_{freeze} \times pd + o_{freeze}) + 1.0)$, where pd is the pulse density of the current patch, and m_{freeze}, s_{freeze} and o_{freeze} are free parameters (multiplicator, slope and offset, respectively). The formula is empirical and was calibrated through a grid search of parameters on three $1\,km^2$ canopy extents at Alice Mulga, Robson Creek and Watts Creek. We here use the most robust parameter set for all subsequent calculations ($m_{freeze} = 3.1$, $s_{freeze} = 1.75$ and $o_{freeze} = 2.1$)

Note: Description of the six algorithms for deriving CHMs tested in the study.
Abbreviations: DSM, digital surface model; DTM, digital terrain model.

algorithms we tested include a simple rasterisation of the highest return per m^2 (CHM$_{highest}$), a TIN-interpolation of first returns (CHM$_{tin}$), a 'pitfree' algorithm that builds the canopy surface by merging multiple TIN-interpolations (CHM$_{pitfree}$, Khosravipour et al., 2014) and the 'spikefree' algorithm, a vertically constrained TIN-interpolation (CHMspikefree, Khosravipour et al., 2016). Both the pitfree and spikefree algorithms were designed to remove or smooth over spurious low points in the canopy ('pits' or 'spikes') that are due to laser pulses penetrating into small (submeter scale) openings, but the two algorithms use different approaches to achieve this (Table 2).

The other two CHM algorithms are newly developed versions of the spikefree algorithm: one that is applied to a thinned-down point cloud (CHM$_{tspikefree}$), and one that adapts the spike-removal to local pulse density variation (CHM$_{lspikefree}$). Both are applied to first returns only and address the problem that pulse densities are typically higher in areas closer to the scanner (centre of flightlines, tall trees, hill tops) and where flightlines overlap, which if uncorrected leads to inconsistencies in height estimates (Roussel et al., 2017). Throughout, we first created digital surface models (DSMs) and obtained CHMs by then subtracting ground heights (DTM based on LAStool's 'lasground_new'). The exception was CHM$_{pitfree}$ which we derived directly from height-normalised point clouds to reduce computation time. A DSM$_{pitfree}$ was constructed post hoc by summing CHM$_{pitfree}$ and DTM.

2.3 | Robustness of CHM generation and forest structure assessments

2.3.1 | Simulating point clouds of varying quality

Pulse density (the number of emitted laser pulses per unit area) is usually the best first-order approximation of airborne laser scan quality, particularly for CHM construction. Pulse density depends on the frequency with which pulses are emitted, but also summarises flightline properties, such as altitude, speed and overlap. It is highest when the laser is flown close to the canopy, at low speed and in narrowly spaced flightlines. As a general rule, the higher the pulse density, the less sensitive is a canopy reconstruction to other laser properties. If, for example, 1 m^2 of canopy is hit by a single shot, it matters a lot where the shot came from, how wide its footprint was, and how the raw energy waveform was converted into a single point (Dayal et al., 2022; Keränen et al., 2016; Roussel et al., 2017, 2018). By contrast, if the same 1 m^2 of canopy is saturated with shots from all directions (e.g. ≥20 pulses m^{-2}), the canopy surface is likely well-approximated irrespective of these properties.

Pulse density is not only an important summary statistic of ALS quality, but also easy to manipulate post hoc through a random (or targeted) thinning of laser shots. Here we used this approach to study how robust CHM algorithms were to variations in point cloud quality. Starting from the high-quality TERN ALS data, we created systematically degraded point clouds with pulse densities of 16, 8, 4, 2, 1 and 0.5 m^{-2} for each of the nine study sites. We used the homogenize() function in the lidR package, which simultaneously thins and homogenises point clouds, so that every grid cell at a target resolution (here 25 m) has the same overall pulse density. We then ran the processing pipeline across the degraded point clouds and created standard DTM and CHM products for further analysis.

While pulse density is the best overall quality indicator, other scan properties can also affect CHMs, particularly at low pulse densities. We therefore carried out three companion analyses: (1) a custom degradation of pulse density that, unlike homogenize(), removed every nth shot, to assess the effects of within-scan heterogeneity; (2) a systematic degradation in laser penetration (i.e. the number of returns per shot) to investigate how higher-order returns affect CHM generation; and (3) a splitting of point clouds into flightlines, which allowed us to study areas of overlap between two flightlines and test whether differences in scan angles between shots from the two flightlines also translated into differences in canopy height estimates between them. For simplicity, we focus on pulse density variation throughout the main text and present the companion analyses in the Supplementary (Sections S2–S4).

2.3.2 | Effects of point cloud quality on CHM generation

The way in which CHM algorithms interpolate laser returns to create canopy surfaces (DSM derivation) is a major source of uncertainty. However, variation is also expected due to errors in ground classification (DTM derivation). For example, at low pulse densities, canopy height could be underestimated because of insufficient sampling of treetops (negative bias in DSM) or insufficient sampling of the ground (positive bias in DTM). We evaluated the two aspects separately: for each site and each pulse density level, we compared both DSMs (one for each algorithm) and DTMs to reference products at the highest pulse density level (16 pulses m^{-2}). Robustness of algorithms was assessed through mean errors (ME, or bias, in m) and root mean square errors (RMSE, in m) of 1 m^2 pixels. Throughout, we visualise DSM/DTM stability across all pulse density levels but only report RMSE and ME for the most extreme but still acceptable point cloud differences (2 vs. 16 pulses m^{-2}). To avoid edge effects, we removed the outer 25 m of all products.

2.3.3 | Effects of point cloud quality on CHM-derived metrics

To assess how pulse density degradation propagated to CHM-derived forest structural metrics, we calculated 25 summary statistics from all CHMs both at 1 ha (100 × 100 m^2) and 1 km^2 (1000 × 1000 m^2) resolution (see Table 3 for details on all metrics). 1 ha is a common size for forest plots and thus an important mapping unit for structural metrics and biomass (Labriere et al., 2018), while 1 km^2 is sufficiently large to sample irregularly distributed canopy features such as large treefall gaps or canopy clusters (Wedeux & Coomes, 2015; Zhang

TABLE 3 Description of the 26 forest structure metrics tested in this study.

Type of metric	Metric	Calculation
Vertical	Mean height (m)	Mean height of CHM pixels
	Median of height (m)	Median height of CHM pixels
	25th/75th/95th/99th percentile of height (m)	Height percentiles of CHM pixels
	SD of height (m)	Standard deviation of CHM pixels
	CV of height	Coefficient of variation of CHM pixels (SD/mean)
	Robust CV of height	Robust CV of CHM pixels (Lobry et al., 2023)
	IQR of height (m)	Interquartile range of CHM pixels
	Canopy cover at 2 and 10 m (%)	Percentage of CHM pixels ≥2 or 10 m in height
Horizontal	Rumple index	Canopy surface area divided by planar area
	Normalised rumple index	Rumple index calculated for a surface that has been normalised by maximum canopy height (99th percentile)
	Moran's I	Spatial autocorrelation, as measured by Moran's I in a $3 \times 3 m^2$ neighbourhood
	Number of clusters <25th percentile of height	The number and mean area of clusters of pixels that lie below the 25th percentile of height and are larger than $25 m^2$. A type of 'gap'. Since gap fraction is fixed at 25%, also applicable at small scales where other thresholds may fail
	Mean size of clusters <25th percentile of height (m^2)	
	Number of clusters >75th percentile of height	The number and mean area of clusters of pixels that lie above the 75th percentile of height and are larger than $25 m^2$. A type of 'crown cluster'. Also applicable at small scales where other thresholds may fail (cf. gaps above)
	Mean size of clusters >75th perc entile of height (m^2)	
	Number of gaps <10 m	The number, mean area and power law slope (λ) of the size frequency distribution of clusters of pixels that lie below a fixed height threshold of 10 m and are larger than $25 m^2$. Only used at $1 km^2$ scale
	Mean size of gaps <10 m (m^2)	
	λ of gaps <10 m	
	Number of gaps <50% mean height	The number, mean area and power law slope (λ) of the size frequency distribution of clusters of pixels below a relative height threshold (50% of mean canopy height) and larger than $25 m^2$. Only used at $1 km^2$ scale
	Mean size of gaps <50% mean height (m^2)	
	λ of gaps <50% mean height	
Derived	Above-ground biomass (Mg ha^{-1})	Above-ground biomass (AGB), predicted from median canopy height (H_{50}) as $AGB = A \times H_{50}{}^{b}$ (Labriere et al., 2018). A and b are fitted for each CHM separately via the AGB of 25 1 ha field inventory plots. Only estimated at the tropical site Robson Creek and only at 1 ha scale

Note: The metrics can be broadly grouped into vertical ones that ignore spatial connections between CHM pixels, and horizontal ones that instead reflect relationships between CHM pixels (1 m^2) and their neighbours. As an additional test, we evaluated above-ground biomass, which requires both CHM and field inventory data for derivation and is thus reported separately. Unless otherwise noted, each metric was calculated at both 1 ha and 1 km^2 scale. We note that we use the power law slope of gap size frequency distributions as an indicator of forest structure, but we did not test whether gap patterns actually conformed to power laws.

Abbreviation: CHM, canopy height model.

et al., 2023). Metrics were grouped into two categories: 'vertical' ones that summarised the height distribution in each grid cell irrespective of spatial associations between the underlying 1 m^2 pixels, and 'horizontal' ones that explicitly assessed the connectivity of the 1 m^2 pixels within each cell. The former included metrics such as the mean, standard deviation, and percentiles of canopy height, while the latter captured spatial autocorrelation (Moran's I), height gradients

(rumple index) and the clumping of canopy structures (gaps below and canopy clusters above height thresholds). We also assessed how robustly the frequency distribution of gap sizes could be inferred at 1 km^2 resolution by using the slope of a power law to describe the relationship between number and size of gaps (Silva et al., 2019). Gaps had to be at least 25 m^2 in size to be included and were defined via a height cut-off, either fixed at 10 m (Silva et al., 2019) or as 50% of

the mean canopy height at $1\,km^2$ resolution (Table 3). Moreover, for one site (tropical forest at Robson Creek) we estimated the impacts of CHM uncertainty and bias on above-ground biomass (AGB) estimation. This was done by regressing field estimates of AGB from 25 1 ha plots against CHM-derived estimates of median canopy height (Labriere et al., 2018). For a more detailed explanation of the AGB analysis see Section S5 of the Supplementary.

For each metric, we again calculated MEs and RMSEs between degraded and reference data sets (2 vs. $16\,m^{-2}$), but now at 1 ha and $1\,km^2$ resolution. To make metrics comparable and assess their utility in deciphering ecological variation, we calculated MEs and RMSEs for each metric and study site separately, and then divided them by the metric's standard deviation either within or across sites (hereafter rMEs and rRMSEs). For the most robust metrics, biases and uncertainties should be dwarfed by biological variation across and within sites (e.g. rMEs $\ll 0.1$ and rRMSEs $\ll 0.2$). To assess the practical effects of mixing high and low-quality point clouds in ecological analyses, we also randomly swapped 50% of cells between 2 and $16\,m^{-2}$ grids (for each site, both at 1 ha and $1\,km^2$ resolution) and calculated Spearman's R^2 between the re-shuffled grids ($R^2_{rankswapped}$). A high $R^2_{rankswapped}$ (>0.9) indicates that forest structure assessments are stable even if low and high pulse densities occur in the same analysis.

2.3.4 | Transferability to other datasets and forest types

To assess the generalisability of our results to woody ecosystems not included in the TERN data (e.g. conifer forests) we identified a second dataset comprising nine highly diverse forest ecosystems from the U.S. for each of which we were able to obtain ALS data covering a spatial extent of $3 \times 3\,km^2$. Using these data, we repeated the main analysis of how pulse density degradation affects the stability of the CHMs and their derived metrics. The site description, methodology and results of this validation analysis are reported in the Supplementary Materials (Section D).

3 | RESULTS

3.1 | Sources of uncertainty and bias in canopy height estimation

Canopy height varied strongly across sites, algorithms and pulse densities (Figures 1 and 2; Tables S4 and S5). When averaged across algorithms, mean canopy height ranged from 2.5 m in the semi-arid acacia woodlands of Alice Mulga to 36.1 m in the wet sclerophyll forests at Watts Creek ($\Delta h = 33.6\,km$). However, values depended strongly on the CHM algorithm: the same sites ranged from 3.4 to 39.7 m for $CHM_{highest}$ ($\Delta h = 36.3\,m$) and from 1.7 to 28.9 m for CHM_{tin} ($\Delta h = 27.2\,m$). The largest relative difference between algorithms at a single site was observed at the savanna site in Litchfield where many

low canopy returns resulted in a mean height of 2.9 m for CHM_{tin}, but 7.3 m for $CHM_{highest}$ (i.e. 2.5 times the value of CHM_{tin}).

Variation in pulse density had a strong effect on canopy height estimates, with decreases from 16 to $2\,m^{-2}$ resulting in a mean absolute bias of up to −5.6 m for tall, wet forests ($CHM_{highest}$ at Watts Creek, or −14% of mean canopy height). In short, open and dry forests, absolute biases were much lower (as low as −0.76 m at Credo) but relative biases reached up to −42% of mean canopy height ($CHM_{pitfree}$ at the acacia woodland of Alice Mulga). RMSEs at pixel-level (i.e. $1\,m^2$ resolution) reached up to 14 m when comparing CHMs generated at 16 versus 2 pulses m^{-2} (Watts Creek, $CHM_{highest}$) and in places exceeded 100% of mean canopy height (savanna site Litchfield, CHM_{tin}). Comparable uncertainties due to within-scan heterogeneity in pulse density were also observed across sites (Figure S5). Most of these errors and uncertainties were due to the CHM algorithms, with little additional effects due to DTM generation (bias ≤0.5 m for most sites). The exception was the tropical rain forest at Robson Creek, where relative changes in canopy height were smaller than for the other sites, dropping by only 3.6 m (13%) from $CHM_{highest}$ to CHM_{tin} and 1.9 m (7%) from 16 to 2 pulses m^{-2} for $CHM_{highest}$. By contrast, Robson Creek exhibited the strongest DTM degradation, with positive biases of 2–5 m at low pulse density, low laser penetration and oblique scan angles (Figure 2; Figure S9; Table S5). Below 2 pulses m^{-2}, deviations between and within CHM algorithms became even more extreme at all sites (Figures 1 and 2; Table S3).

3.2 | Robustness of CHM algorithms

Among the six algorithms we tested, $CHM_{lspikefree}$ was the most robust to degradation in pulse density, followed by CHM_{tin}, with both showing little degradation between 16 and 2 pulses m^{-2}, even in tall canopies (maximum bias of −0.52 and +0.57 m respectively, Table S3). However, between the two, CHM_{tin} was much noisier than $CHM_{lspikefree}$, which had the overall lowest RMSEs (Figure 1; Table S3). Deviations in the other four algorithms were variable, but typically much larger (Table S3). For example, at 2 pulses m^{-2}, height biases in two commonly used CHM types ($CHM_{highest}$ and $CHM_{pitfree}$) routinely reached several metres. In addition, $CHM_{highest}$ degraded rapidly in coverage (~4% NA values at 2 pulses m^{-2}, ~42% at $0.5\,m^{-2}$). A visual assessment of algorithms confirmed the highest consistency in $CHM_{lspikefree}$ and the clearest degradation in $CHM_{highest}$ (Figure 1; Figures S1–S4). However, it also showed that, at high pulse densities, contours were sharper in $CHM_{highest}$ and $CHM_{spikefree}$ than in CHM_{tin} (too noisy) and $CHM_{lspikefree}$ (too smooth).

We obtained very similar results when applying the various CHM algorithms to the second dataset of nine sites from the United States, indicating that $CHM_{lspikefree}$ and CHM_{tin} are able to generate robust surface models across a wide range of forest types and scanning configurations (Supplementary Material R1 and Table R2). Moreover, the results focused on pulse density modulation were
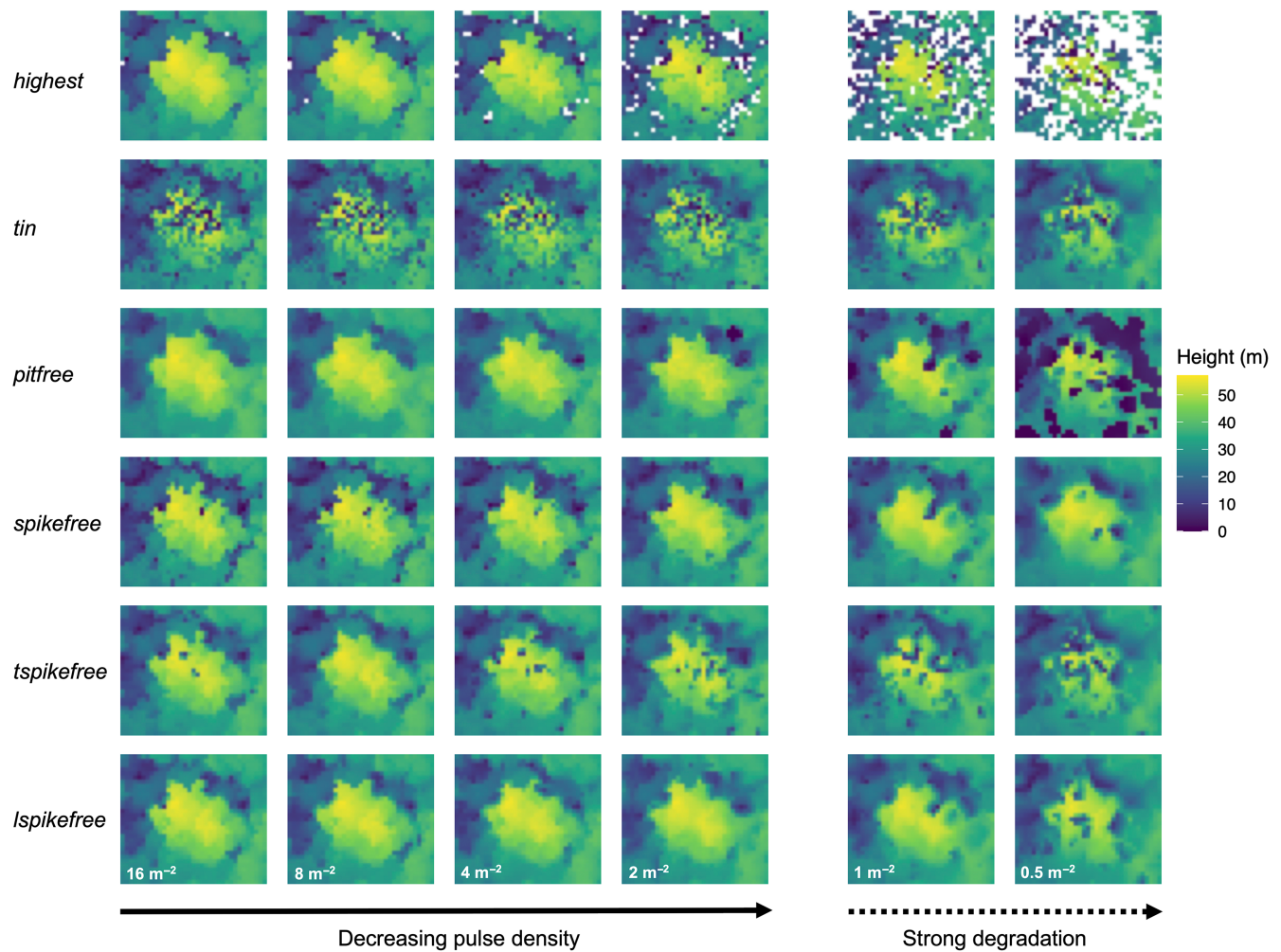
FIGURE 1 Canopy height models across pulse densities for a single tree at Robson Creek. Shown are canopy height models (CHMs, 1-m^2 resolution) for a tree at Robson Creek (crown diameter = 23 m) from 16 down to 0.5 pulses m^{-2}. Each row corresponds to a CHM algorithm. Algorithms degrade severely below 2 pulses m^{-2}, which is why robustness was assessed only above this sampling threshold (see Figures S1–S4 for a visualisation of CHMs for different types of degradations and sites).

consistent with companion analyses of scan angle and laser penetration, where CHM$_{lspikefree}$-based estimates also came out as the most robust, closely followed by CHM$_{tin}$ (Table S3). However, even for CHM$_{lspikefree}$ and CHM$_{tin}$, canopy height was systematically underestimated at larger scan angles (site-dependent biases ranging from 0.0 to −1.12 m and from −0.09 to −1.05 m, respectively, for scan angle increases of 15° or more; Table S3; Figure S4).

3.3 | Robustness of CHM-derived forest structure metrics

Downstream analyses were strongly affected by errors in CHM creation. We compared the calculation of a total of 25 metrics between 2 and 16 pulses m^{-2} at both 1 ha and 1 km^2 scales (see Figure 3 for examples, and Figures S10–S23 for a full overview), and RMSEs and MEs often reached or exceeded the standard deviation of the target variables within sites (rRMSE of 50%–100% or more; Tables S6

and S7). In a few cases, errors and biases even exceeded cross-site variation by a factor of 2 or more, and some metrics never reached $R^2_{rankswapped} > 0.9$ within sites even in comparisons between high-quality scans, indicating an inherent instability in those metrics (Table S12).

However, there were clear differences between CHM algorithms and between vertical and horizontal metrics. CHM$_{lspikefree}$ and CHM$_{tin}$ were the most robust, with CHM$_{lspikefree}$ performing slightly better. It had low rRMSEs and rMEs for all vertical metrics (<10% across sites and 10%–20% within sites; Tables S6–S9) and highly conserved rankings when randomly combining measurements at low and high pulse densities ($R^2_{rankswapped} \sim 1.00$ across and $R^2_{rankswapped} \sim 0.90$–0.95 within sites; Tables S10 and S11; Figures S10–S23). The consistency of CHM$_{lspikefree}$-inferred vertical metrics translated to derived products, such as above-ground biomass (AGB; Figure 3; Table S12). Errors due to pulse density degradation (16.1 Mg ha^{-1}) were small compared to those of other algorithms such as CHM$_{highest}$ and CHM$_{pitfree}$ (49.2 and
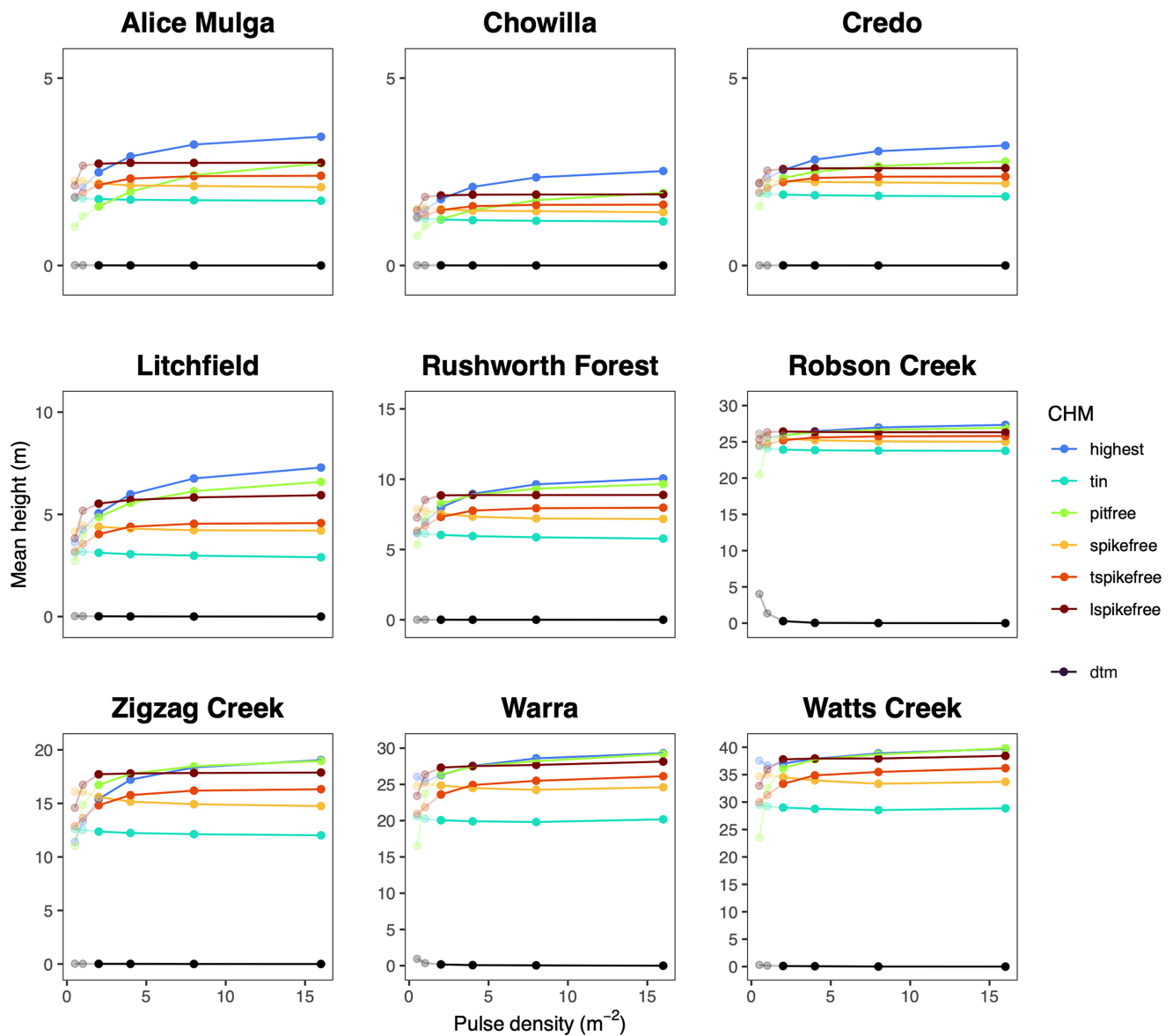
FIGURE 2 Changes in mean canopy height across pulse densities and algorithms for all TERN SuperSites. Shown is mean canopy height from 0.5 to 16 pulses m^{-2} across canopy height model (CHM) algorithms and study sites. To separate out effects on topography from effects on canopy surfaces, CHMs are computed by subtracting a reference digital terrain model (DTM) generated using high-quality point clouds (16 pulses m^{-2}) from digital surface models generated using increasingly degraded point clouds. Also shown is a pulse-density specific DTM (black line), normalised by the reference DTM of each site. Changes below 2 pulses m^{-2} are plotted with transparency, as they were not used for robustness assessments. Figures S7 and S8 show the equivalent for laser penetration degradation and scan angle differences.

34.2 Mg ha^{-1}, respectively), errors in the biomass models themselves (41.9 Mg ha^{-1}) and the mean biomass across the entire area (483.3 Mg ha^{-1}). Horizontal metrics were also the most robust when derived from CHM$_{lspikefree}$, but showed considerable errors and uncertainties within sites (50%–100% rRMSE and rME; $R^2_{rankswapped}$ of 0.3–0.7). An exception were canopy gap statistics, when gaps were defined as clusters of pixels that lie below 50% of the mean canopy height at 1 km^2 resolution. For CHM$_{lspikefree}$, their number, mean size and power law slopes were well-preserved across (rRMSEs ~10% and rMEs ~5%) and within sites (~25% and 10%).

CHM$_{tin}$-derived metrics were also robust, and for some metrics (e.g. upper percentiles of height), all algorithms performed well. But CHM$_{lspikefree}$ was more consistent overall and the only algorithm for which at least some horizontal metrics had within-site rRMSEs below 40% and $R^2_{rankswapped} > 0.9$ (Tables S7 and S11). On the other hand, two commonly used algorithms, CHM$_{highest}$ and CHM$_{pitfree}$, were consistently the worst-performing, with errors regularly exceeding 100% and rank-consistency <0.9 for most metrics (Tables S10 and S11). The same patterns were found in our replication study in U.S. forests (Tables R3–R8).
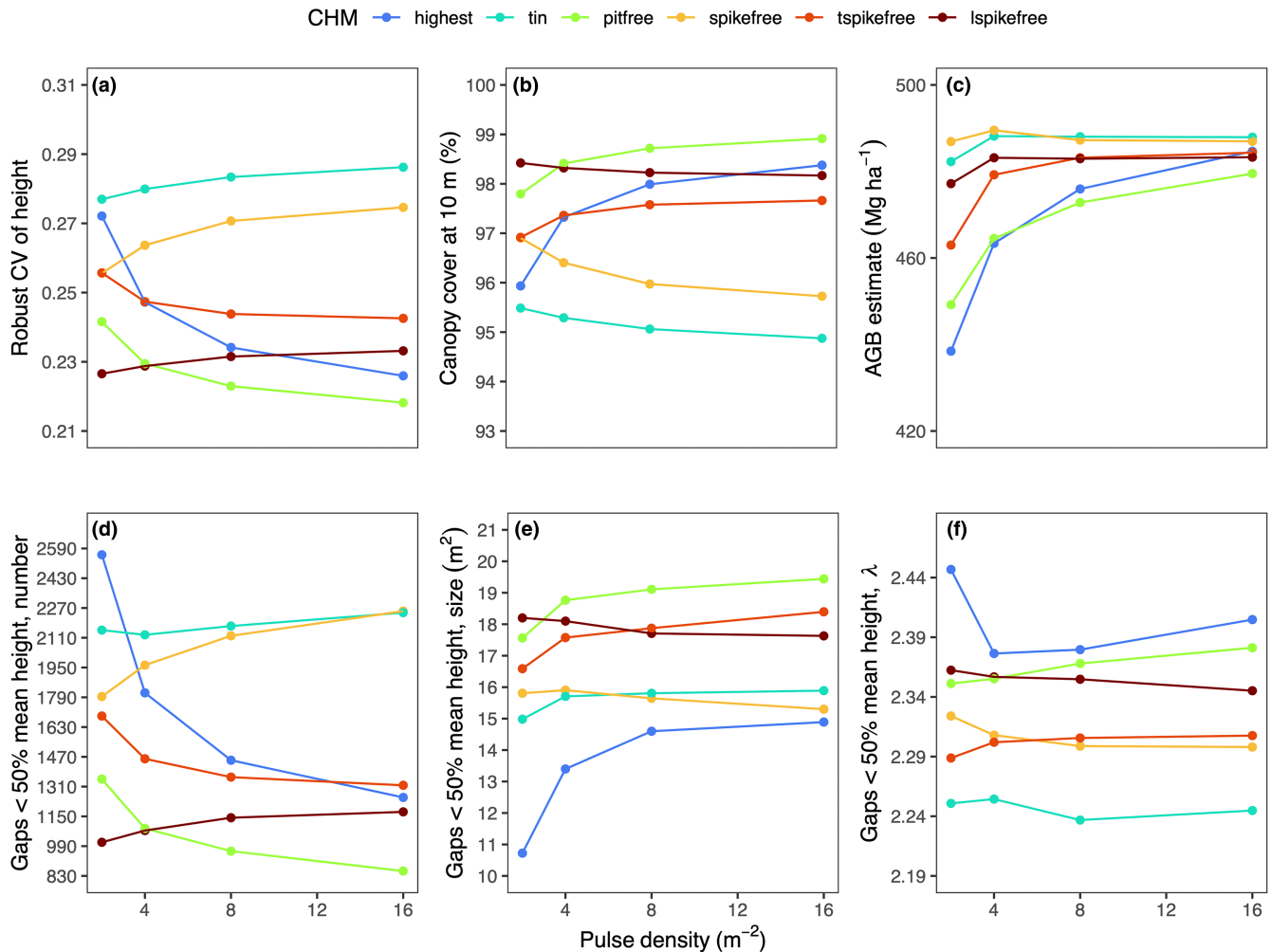
FIGURE 3 Robustness of CHM-derived structural metrics at Robson Creek under point cloud degradation. Shown are a selection of six measures of forest structure. The top row shows vertical metrics and those derived from them, including (a) the robust coefficient of variation (Lobry et al., 2023) of height, (b) canopy cover at 10 m above-ground and (c) above-ground biomass (AGB), all estimated at 1 ha resolution. The bottom row shows horizontal metrics calculated at $1 km^2$ resolution, including the number (d), average size (e) and power law slope (f) of gaps, where gaps are defined as clusters of all $1 m^2$ pixels <50% of mean canopy height and $>25 m^2$ in total area. We rescaled tick marks on the *y*-axis to correspond to 50% of each metric's typical standard deviation at 16 pulses m^{-2}. Biases smaller than inter-tick mark distance thus indicate robustness, while those exceeding it denote instability.

4 | DISCUSSION

Laser scanning technology is advancing fast, and ALS data are increasingly available in huge, open archives (e.g. https://opentopography.org/). This presents a unique opportunity for ecologists to characterise ecosystems in time (Huertas et al., 2022) and in space (Jucker, 2022). In particular, ALS-derived CHMs hold a lot of promise, as they are easy to create, share and interpret, more robust than point cloud-derived metrics (Mielcarek et al., 2018; Zhang et al., 2024) and a core part of most point cloud processing tools (Roussel et al., 2020). ALS-derived CHMs already play a key role in the validation and calibration both of regional forest structure products (Wagner et al., 2024) and of global satellite-derived products (Duncanson et al., 2022; Lang et al., 2023; Tolan et al., 2024). Moreover, as multi-temporal ALS data become increasingly available, CHMs will allow the fine-scale monitoring of forest dynamics

at large spatial scales—making it imperative that we develop robust approaches for generating them.

Using high-quality ALS data from nine TERN SuperSites in Australia that span a wide range of forest types, we show that many of the ecological metrics we typically derive from ALS (e.g. height, gaps, AGB) are highly susceptible to the choice of CHM algorithm. We found that estimates of forest structure vary widely both between CHM algorithms and for the same algorithm under different degrees of point cloud degradation. However, robust assessments of canopy structure are possible through careful methodological choices. As a way forward, we present a new type of CHM that improves the robustness of an existing algorithm (Khosravipour et al., 2016). We accompany this with an openly available pipeline to derive and compare these CHMs in R, and a set of 16 best-practice guidelines that will allow ecologists to make the most of growing access to ALS data (Figure 4).

FIGURE 4 Sixteen simple guidelines for robust forest structure analysis. Shown are best-practice guidelines for robust assessments of forest structure from airborne laser scanning via canopy height models (CHMs). We assume that (a) scans have been acquired at pulse densities high enough to produce accurate ground models, (b) the target resolution for CHMs is 1 m and (c) that the aim is to compare forest structural properties across scans and sites. For some goals, such as tree crown delineation across a single high-quality scan, other algorithms such as CHM$_{highest}$ or CHM$_{spikefree}$ may prove useful.

16 SIMPLE GUIDELINES FOR ROBUST FOREST STRUCTURE ANALYSIS

Laser scan quality

1) Mask areas with <2 pulses m^{-2}
2) Mask areas with <4 pulses m^{-2} on densely vegetated and steep terrain
3) Mask areas with scan angles >20°
4) Visually check for systematic biases (e.g. higher pulse densities on hilltops and emergent tree crowns)

Canopy height models

5) Only use 1st returns for creating CHMs
6) Use algorithms that adapt to local pulse density variation
7) Use CHM$_{lspikefree}$ for best results and CHM$_{tin}$ for simplicity and speed
8) Avoid combining and comparing CHMs generated with different algorithms

Structural metrics

9) Choose simple and interpretable metrics over complex ones
10) Choose metrics that are robust to differences in CHMs and point clouds
11) Confidently use vertical (height) metrics at any scale
12) Use horizontal (connectivity) metrics cautiously, ideally at scales >1000 m

Ecological inference

13) Control for variation in local pulse density in models
14) Include scanning season as a covariate to control for phenology and snow
15) Check if effect sizes are larger than the uncertainty in the structural metrics
16) Repeat analyses using a second robust CHM algorithm

4.1 | Not all canopy height models are created equal…

A clear takeaway from our analysis is that canopy height cannot be compared across CHM algorithms and that variation in point cloud properties adds large errors. Mean canopy height estimates could differ by up to 10 m between algorithms and up to 60% in relative height, and point cloud degradation added biases of up to ~5 m, or up to ~40% in relative terms. This is true even when staying within reasonable quality ranges (e.g. densities ≥2 pulses m^{-2}) and despite the general robustness of CHMs to differences in light extinction and good retrieval of top canopy height (Mielcarek et al., 2018). To make matters worse, errors were inconsistent across sites—higher absolute errors in tall, higher relative errors in short forests (Table S3)—and within scans (Figure S5; Table S3). Large scan angle differences (15–20°) also introduced a negative bias in height estimates, but across-scan pulse density variation was the single most important factor in determining CHM quality, in agreement with previous studies that found similar effects of pulse or return densities (e.g. LaRue et al., 2022).

Errors and uncertainties in CHM algorithms had disproportionately large effects on derived structural metrics, often exceeding ecological variation within sites. For extremely sensitive metrics (Moran's *I* or gap statistics from CHM$_{highest}$), errors and uncertainties even exceeded variation across the entire gradient from open Acacia woodlands to 90-m tall Mountain Ash forests. This is beyond most ranges seen in ecological studies and, barring stand-replacing disturbance, exceeds forest dynamics by orders of magnitude. Even at a single site (Robson Creek) and for a comparatively robust definition of canopy gaps (clusters of pixels <50% of mean height and >25 m^2 in size), values ranged from ~800 to ~2200 gaps km^{-2} between algorithms, and could go from ~1200 to ~2600 gaps km^{-2} across pulse

densities for a single algorithm (CHM$_{highest}$). In comparison, estimates of above-ground biomass were more stable, but degradation in pulse density could still lead to biases in excess of model calibration errors (~50 Mg ha^{-1} for CHM$_{highest}$) and >10% of the landscape-level estimates (~485 Mg ha^{-1}).

4.2 | … but we can make them more equal

There is, however, a clear way forward when it comes to implementing robust high-resolution (1 m^2) forest structure assessments (see Figure 4 for a condensed version). As a general rule, we recommend masking areas below 2 pulses m^{-2} (averaged at 5–10 m) and below 4 m^{-2} in rugged terrain with dense vegetation (see degradation in Figures 1 and 2; Figure S9). The effects of scan angle variation and laser penetration were small relative to those of pulse density (Figure S4), but became noticeable at 15–20°, so we recommend 20° as upper limit (see Dayal et al., 2022). Masking of areas is also recommended when DTMs cannot be reliably inferred due to a lack of ground returns.

Second, forest structural estimates should be derived from a single, consistent CHM, ideally one that uses only first returns and adapts to pulse density variation. Two of our algorithms fulfilled these criteria (CHM$_{lspikefree}$ and CHM$_{tin}$). CHM$_{lspikefree}$, an algorithm that we developed as part of this study as a refinement to the pre-existing 'spikefree' algorithm (Khosravipour et al., 2016), had the lowest errors across metrics (<5% of across-site variation). It also preserved most canopy properties when mixing scans from high and low pulse densities ($R^2_{rankswapped}$ = 0.95–1.0 across and within sites) and was the only algorithm that estimated gap statistics with reasonable accuracy (rRMSE ~25% within sites). CHM$_{tin}$, a much simpler Delaunay-triangulation of first returns, matched the

low biases in CHM$_{\text{lspikefree}}$, but created noisy and porous canopy surfaces. The application of CHM$_{\text{tin}}$ is thus context-dependent—better for estimating light-penetration, worse for estimating top height—but it offers a useful complement to CHM$_{\text{lspikefree}}$. In contrast, two of the most commonly used algorithms, CHM$_{\text{highest}}$ and CHM$_{\text{pitfree}}$, performed badly throughout. We recommend their application only in specific cases, such as when sample areas are scanned with the same instruments or at high densities (>20 pulses m^{-2}).

Third, for most applications we recommend using statistics that summarise the vertical distribution of canopy elements, such as the mean, standard deviation or percentiles of canopy height. Vertical metrics are simple to calculate and interpret, robust and have been successfully used for the modelling and mapping of forest plot attributes (Pearse et al., 2019; Tompalski et al., 2019; Wilkes et al., 2015). In contrast, horizontal metrics that quantify the connectivity of CHM pixels—spatial autocorrelation, height gradients and canopy features such as gaps or other types of canopy pixel clusters—are less robust. They are attractive, because they open up many ecological questions around canopy dynamics and biodiversity (Asner, Kellner, et al., 2013; Jucker, 2022). However, they are difficult to interpret and proved extremely volatile, with only a single gap definition (clusters of pixels <50% of mean canopy height) producing moderately reliable statistics, and only for the most robust algorithm at the largest spatial scale (CHM$_{\text{lspikefree}}$ at 1 km^2).

Finally, any measurement will involve some form of error. Even the most robust algorithms, such as CHM$_{\text{lspikefree}}$ and CHM$_{\text{tin}}$, showed small biases in this study, and some features of ALS data (e.g. footprint size, or acquisition timing and its relation to phenology or snow cover) were difficult to correct for. We therefore recommend including summaries of point cloud quality (pulse densities and scan angles) and ecological confounders of structure (e.g. vegetation indices that reflect phenology) into statistical models. Crucially, effect sizes should always be put into context of the typical noise and biases of CHMs and derived metrics. Differences <1.0 m in canopy height, for example, should be interpreted with great caution. When in doubt, it may be useful to repeat analyses with a second type of CHM.

4.3 | Towards a robust analysis of forest canopies at global scales

Our study provides a systematic assessment of the robustness of six different CHM algorithms and derived forest structure metrics under point cloud degradation. Our results hold across a broad range of forest types, but their interpretation may vary in specific research contexts and study systems. For one, there are several caveats: we ignored interactions between pulse density degradation and other sources of uncertainty (e.g. an operator flying at higher altitudes can compensate lower return densities by increasing laser power) and focussed on sites with relatively flat terrain, except for the tropical forests at Robson Creek (Figure S9). Furthermore, some sources of

point cloud variation (e.g. rotational patterns of scanners, varying footprint sizes or waveform-to-discrete-point conversion) were beyond the scope of our analysis due to the systematic scanning set-up at the TERN SuperSites. Robustness assessments of these properties and how they interact would require further investigation with different instruments and software as well as flights at different altitudes (Boucher et al., 2023; Brede et al., 2022; Næsset, 2009). Footprint size, for example, has been found to introduce moderate (0.1–0.5 m) but variable biases into height estimates that include both positive (Næsset, 2009), negative (Morsdorf et al., 2008; Roussel et al., 2017) and site-dependent (Goodwin et al., 2006) shifts when comparing small and large footprints. However, properties such as footprint size are often inconsistently reported, and their effects generally diminish as pulse density and sampling of the canopy increases. Therefore, pulse density, an inherent feature of ALS point clouds, provides the best first-order correction for forest structure analysis.

Second, if a study relies on a single scan or a set of scans with the same sampling design, some of our rules-of-thumb could be relaxed. For example, to estimate tree top heights (generally the most robust, Tables S10 and S11), it might be advantageous to retain pulse densities <2 m^{-2} and maximise information by using CHMs based on all returns (Mielcarek et al., 2018). Similarly, one could use the sharper contours of CHM$_{\text{highest}}$ or CHM$_{\text{spikefree}}$ for tree crown delineation together with targeted height corrections (Roussel et al., 2017). It may even sometimes make sense to use unstable metrics such as the rumple index, as there is an accuracy-robustness trade-off: many metrics are unstable precisely because they are sensitive to fine-scale variation in point cloud distributions. For high-quality scans—such as modern, large-scale surveys that easily reach densities of 50–100 pulses m^{-2} (McNicol et al., 2021)—these metrics may provide a lot of ecological information in return for only small biases. However, there are caveats: most scans in open archives (e.g. https://opentopography.org/) have both low and spatially variable pulse densities and even high-quality scans can vary strongly in pulse density (Figure S5). Moreover, some metrics such as Moran's I may be so inherently noisy or bias-prone that they should be generally avoided (substantial differences even between 8 and 16 pulses m^{-2}; Table S10). Finally, any use of non-robust metrics limits comparability across studies and precludes investigations of temporal change.

Third, while the nine TERN SuperSites in Australia cover a wide range of forest structural types—from semi-arid shrublands all the way to dense tropical rainforests—they cannot be representative of all forest ecosystems. To address the lack of conifer or mixed forest types in this dataset, we carried out a replication test with ALS data from nine additional US sites (Supplementary Material, Section D). The replication sites included a wide range of ecosystems with an emphasis on conifer forests—including subtropical pine forests in Florida, redwoods in California, temperate montane forests in the Pacific Northwest and boreal black spruce forests in Alaska (Table R1)—and showed the same patterns as the TERN SuperSites. We again found clear biases at low pulse densities in two commonly

used CHM algorithms ($CHM_{highest}$ and $CHM_{pitfree}$), an increase in absolute biases with canopy height and a much larger sensitivity to pulse density among horizontal than vertical metrics. But we also again found high robustness in $CHM_{lspikefree}$ and CHM_{tin}, particular for vertical forest structure metrics. Overall, this suggests that our general recommendations are applicable across ecosystems globally.

Finally, our study does not provide an exhaustive picture of all potential metrics that can be derived from ALS. In the future, we might be able to derive more robust metrics or develop more stable CHM algorithms. Crucially, our analysis also does not peek below the canopy surface, but this is where a lot of important ecological processes are happening. Expanding our robustness analysis to point cloud or voxel-derived metrics (Pearse et al., 2019; Vincent et al., 2023) is a priority, and the current developments are exciting. Several recent studies systematically assessed how point cloud and instrument properties propagate to the measurement of ecologically interesting features (Dayal et al., 2022; LaRue et al., 2022; Roussel et al., 2017, 2018; Tompalski et al., 2019; Vincent et al., 2023). It is through studies such as these that ecology will be able to separate out scanning artefacts and noise from biological variation. This creates a secure foundation for the quantification and monitoring of fine-scale canopy and carbon dynamics, microclimates and animal habitats at global scales.

AUTHOR CONTRIBUTIONS

Fabian Jörg Fischer and Tommaso Jucker conceived of the study. Toby Jackson and Grégoire Vincent contributed critically to the analysis and to the writing of the draft. Fabian Jörg Fischer led the development of algorithms, writing and analysis of the data, with substantial inputs from all co-authors.

ACKNOWLEDGEMENTS

CONFLICT OF INTEREST STATEMENT

The authors declare no conflict of interest.

PEER REVIEW

The peer review history for this article is available at https://www.webofscience.com/api/gateway/wos/peer-review/10.1111/2041-210X.14416.

DATA AVAILABILITY STATEMENT

All data used in this study are openly available on the Terrestrial Ecosystem Research Network's homepage: ALS data at https://portal.tern.org.au/metadata/TERN%2F4ff0b4c9-cfa0-4d09-9520-b5402 adc583f (Department of Environment and Science, 2021) and field data for Robson Creek at https://portal.tern.org.au/metadata/super site.174 (Bradford et al., 2024). All R scripts, including the ALS processing pipeline and functions used for analysis and visualisation, as well as derived products that support the results in the article are available on Zenodo at http://doi.org/10.5281/zenodo.10878070 (Fischer et al., 2024a). A replication analysis can also be found at https://doi.org/10.5281/zenodo.13148966 (Fischer et al., 2024b).

ORCID

Fabian Jörg Fischer https://orcid.org/0000-0003-2325-9886
Toby Jackson https://orcid.org/0000-0001-8143-6161
Grégoire Vincent https://orcid.org/0000-0001-9443-021X
Tommaso Jucker https://orcid.org/0000-0002-0751-6312

REFERENCES

Alkama, R., & Cescatti, A. (2016). Biophysical climate impacts of recent changes in global forest cover. *Science*, 351(6273), 600–604. https://doi.org/10.1126/science.aac8083

Almeida, D. R. A. d., Stark, S. C., Shao, G., Schietti, J., Nelson, B. W., Silva, C. A., Gorgens, E. B., Valbuena, R., Papa, D. d. A., & Brancalion, P. H. S. (2019). Optimizing the remote detection of tropical rainforest structure with airborne Lidar: Leaf area profile sensitivity to pulse density and spatial sampling. *Remote Sensing*, 11(1), 92. https://doi.org/10.3390/rs11010092

Andrade, M. S., Gorgens, E. B., Reis, C. R., Cantinho, R. Z., Assis, M., Sato, L., & Ometto, J. P. H. B. (2018). Airborne laser scanning for terrain modeling in the Amazon forest. *Acta Amazonica*, 48(4), 271–279. https://doi.org/10.1590/1809-4392201800132

Asner, G. P., Kellner, J. R., Kennedy-Bowdoin, T., Knapp, D. E., Anderson, C., & Martin, R. E. (2013). Forest canopy gap distributions in the southern Peruvian Amazon. *PLoS One*, 8(4), e60875. https://doi.org/10.1371/journal.pone.0060875

Asner, G. P., Mascaro, J., Anderson, C., Knapp, D. E., Martin, R. E., Kennedy-Bowdoin, T., van Breugel, M., Davies, S., Hall, J. S., Muller-Landau, H. C., Potvin, C., Sousa, W., Wright, J., & Bermingham, E. (2013). High-fidelity national carbon mapping for resource management and REDD+. *Carbon Balance and Management*, 8(1), 7. https://doi.org/10.1186/1750-0680-8-7

Atkins, J. W., Fahey, R. T., Hardiman, B. S., & Gough, C. M. (2018). Forest canopy structural complexity and light absorption relationships at the subcontinental scale. *Journal of Geophysical Research: Biogeosciences*, 123(4), 1387–1405. https://doi.org/10.1002/2017JG004256

Aubry-Kientz, M., Dutrieux, R., Ferraz, A., Saatchi, S., Hamraz, H., Williams, J., Coomes, D., Piboule, A., & Vincent, G. (2019). A comparative assessment of the performance of individual tree crowns delineation algorithms from ALS data in tropical forests. *Remote Sensing*, 11(9), 1086. https://doi.org/10.3390/rs11091086

Baker, P. J., & Wilson, J. S. (2000). A quantitative technique for the identification of canopy stratification in tropical and temperate forests. *Forest Ecology and Management*, 127(1–3), 77–86. https://doi.org/10.1016/S0378-1127(99)00118-8

Bottalico, F., Chirici, G., Giannini, R., Mele, S., Mura, M., Puxeddu, M., McRoberts, R. E., Valbuena, R., & Travaglini, D. (2017). Modeling Mediterranean forest structure using airborne laser scanning data. *International Journal of Applied Earth Observation and Geoinformation*, 57, 145–153. https://doi.org/10.1016/j.jag.2016.12.013

Boucher, P. B., Hockridge, E. G., Singh, J., & Davies, A. B. (2023). Flying high: Sampling savanna vegetation with UAV-lidar. *Methods in*

Ecology and Evolution, 14(7), 1668–1686. https://doi.org/10.1111/2041-210X.14081

Bradford, M., McKeown, A., Ford, A., & Liddell, M. (2024). *Robson Creek rainforest diameter, height and aboveground Woody biomass data.* Version 1.0. Terrestrial Ecosystem Research Network (Dataset). https://portal.tern.org.au/metadata/TERN/5a864ec1-f780-4104-a242-7ff00e1f4962

Brede, B., Bartholomeus, H. M., Barbier, N., Pimont, F., Vincent, G., & Herold, M. (2022). Peering through the thicket: Effects of UAV LiDAR scanner settings and flight planning on canopy volume discovery. *International Journal of Applied Earth Observation and Geoinformation*, 114, 103056. https://doi.org/10.1016/j.jag.2022.103056

Chen, Z., Gao, B., & Devereux, B. (2017). State-of-the-art: DTM generation using airborne LIDAR data. *Sensors*, 17(1), 150. https://doi.org/10.3390/s17010150

Coomes, D. A., Asner, G. P., Lewis, S. L., Dalponte, M., Phillips, O. L., Qie, L., Nilus, R., Phua, M.-H., Banin, L. F., Burslem, D. F. R. P., & Jucker, T. (2017). Area-based vs tree-centric approaches to mapping forest carbon in southeast Asian forests from airborne laser scanning data. *Remote Sensing of Environment*, 194, 77–88. https://doi.org/10.1016/j.rse.2017.03.017

Dalagnol, R., Wagner, F. H., Galvão, L. S., Streher, A. S., Phillips, O. L., Gloor, E., Pugh, T. A. M., Ometto, J. P. H. B., & Aragão, L. E. O. C. (2021). Large-scale variations in the dynamics of Amazon forest canopy gaps from airborne lidar data and opportunities for tree mortality estimates. *Scientific Reports*, 11(1), 1388. https://doi.org/10.1038/s41598-020-80809-w

Davies, A. B., & Asner, G. P. (2014). Advances in animal ecology from 3D-LiDAR ecosystem mapping. *Trends in Ecology & Evolution*, 29(12), 681–691. https://doi.org/10.1016/j.tree.2014.10.005

Dayal, K. R., Durrieu, S., Lahssini, K., Alleaume, S., Bouvier, M., Monnet, J.-M., Renaud, J.-P., & Revers, F. (2022). An investigation into lidar scan angle impacts on stand attribute predictions in different forest environments. *ISPRS Journal of Photogrammetry and Remote Sensing*, 193, 314–338. https://doi.org/10.1016/j.isprsjprs.2022.08.013

De Frenne, P., Lenoir, J., Luoto, M., Scheffers, B. R., Zellweger, F., Aalto, J., Ashcroft, M. B., Christiansen, D. M., Decocq, G., De Pauw, K., Govaert, S., Greiser, C., Gril, E., Hampe, A., Jucker, T., Klinges, D. H., Koelemeijer, I. A., Lembrechts, J. J., Marrec, R., … Hylander, K. (2021). Forest microclimates and climate change: Importance, drivers and future research agenda. *Global Change Biology*, 27(11), 2279–2297. https://doi.org/10.1111/gcb.15569

Department of Environment and Science, Q. G. (2021). *Airborne hyperspectral and LiDAR data—Australian field sites*. Version 1.0. Terrestrial Ecosystem Research Network (Dataset). https://portal.tern.org.au/metadata/TERN/4ff0b4c9-cfa0-4d09-9520-b5402adc583f

Dowle, M., & Srinivasan, A. (2023). *data.table: Extension of 'data.frame'.* https://CRAN.R-project.org/package=data.table

Duncanson, L., Kellner, J. R., Armston, J., Dubayah, R., Minor, D. M., Hancock, S., Healey, S. P., Patterson, P. L., Saarela, S., Marselis, S., Silva, C. E., Bruening, J., Goetz, S. J., Tang, H., Hofton, M., Blair, B., Luthcke, S., Fatoyinbo, L., Abernethy, K., … Zgraggen, C. (2022). Aboveground biomass density models for NASA's Global Ecosystem Dynamics Investigation (GEDI) lidar mission. *Remote Sensing of Environment*, 270, 112845. https://doi.org/10.1016/j.rse.2021.112845

Ehbrecht, M., Seidel, D., Annighöfer, P., Kreft, H., Köhler, M., Zemp, D. C., Puettmann, K., Nilus, R., Babweteera, F., Willim, K., Stiers, M., Soto, D., Boehmer, H. J., Fisichelli, N., Burnett, M., Juday, G., Stephens, S. L., & Ammer, C. (2021). Global patterns and climatic controls of forest structural complexity. *Nature Communications*, 12(1), 519. https://doi.org/10.1038/s41467-020-20767-z

Felipe-Lucia, M. R., Soliveres, S., Penone, C., Manning, P., van der Plas, F., Boch, S., Prati, D., Ammer, C., Schall, P., Gossner, M. M., Bauhus, J., Buscot, F., Blaser, S., Blüthgen, N., de Frutos, A., Ehbrecht, M.,

Frank, K., Goldmann, K., Hänsel, F., … Allan, E. (2018). Multiple forest attributes underpin the supply of multiple ecosystem services. *Nature Communications*, 9(1), 4839. https://doi.org/10.1038/s41467-018-07082-4

Fischer, F. J., Jackson, T., Vincent, G., & Jucker, T. (2024a). Data for article: Robust characterization of forest structure from airborne laser scanning—A systematic assessment and sample workflow for ecologists. *Zenodo*, https://doi.org/10.5281/zenodo.10878070

Fischer, F. J., Jackson, T., Vincent, G., & Jucker, T. (2024b). Supplementary data for article: Robust characterization of forest structure from airborne laser scanning—A systematic assessment and sample workflow for ecologists. *Zenodo*, https://doi.org/10.5281/zenodo.13148966

Fischer, F. J., & Jucker, T. (2024). No evidence for fractal scaling in canopy surfaces across a diverse range of forest types. *Journal of Ecology*, 112, 470–486. https://doi.org/10.1111/1365-2745.14244

Fischer, F. J., Labrière, N., Vincent, G., Hérault, B., Alonso, A., Memiaghe, H., Bissiengou, P., Kenfack, D., Saatchi, S., & Chave, J. (2020). A simulation method to infer tree allometry and forest structure from airborne laser scanning and forest inventories. *Remote Sensing of Environment*, 251, 112056. https://doi.org/10.1016/j.rse.2020.112056

Fischer, R., Knapp, N., Bohn, F., Shugart, H. H., & Huth, A. (2019). The relevance of forest structure for biomass and productivity in temperate forests: New perspectives for remote sensing. *Surveys in Geophysics*, 40(4), 709–734. https://doi.org/10.1007/s10712-019-09519-x

Goodbody, T. R. H., Tompalski, P., Coops, N. C., White, J. C., Wulder, M. A., & Sanelli, M. (2020). Uncovering spatial and ecological variability in gap size frequency distributions in the Canadian boreal forest. *Scientific Reports*, 10(1), 6069. https://doi.org/10.1038/s41598-020-62878-z

Goodwin, N. R., Coops, N. C., & Culvenor, D. S. (2006). Assessment of forest structure with airborne LiDAR and the effects of platform altitude. *Remote Sensing of Environment*, 103(2), 140–152. https://doi.org/10.1016/j.rse.2006.03.003

Gouveia, S. F., Villalobos, F., Dobrovolski, R., Beltrão-Mendes, R., & Ferrari, S. F. (2014). Forest structure drives global diversity of primates. *Journal of Animal Ecology*, 83(6), 1523–1530. https://doi.org/10.1111/1365-2656.12241

Hijmans, R. J. (2023). *terra: Spatial data analysis*. https://CRAN.R-project.org/package=terra

Huertas, C., Sabatier, D., Derroire, G., Ferry, B., Jackson, T. D., Pélissier, R., & Vincent, G. (2022). Mapping tree mortality rate in a tropical moist forest using multi-temporal LiDAR. *International Journal of Applied Earth Observation and Geoinformation*, 109, 102780. https://doi.org/10.1016/j.jag.2022.102780

Isenburg, M. (2023). *LAStools—Efficient LiDAR processing software*. rapidlasso GmbH.

Jackson, T., Fischer, F. J., Vincent, G., Gorgens, E., Keller, M., Chave, J., Jucker, T., & Coomes, D. (2024). Tall Bornean forests experience higher canopy disturbance rates than the eastern Amazon or Guiana shield. *Global Change Biology* (in press). https://doi.org/10.1111/gcb.17493

Jucker, T. (2022). Deciphering the fingerprint of disturbance on the three-dimensional structure of the world's forests. *New Phytologist*, 233(2), 612–617. https://doi.org/10.1111/nph.17729

Kaartinen, H., Hyyppä, J., Yu, X., Vastaranta, M., Hyyppä, H., Kukko, A., Holopainen, M., Heipke, C., Hirschmugl, M., Morsdorf, F., Næsset, E., Pitkänen, J., Popescu, S., Solberg, S., Wolf, B. M., & Wu, J.-C. (2012). An international comparison of individual tree detection and extraction using airborne laser scanning. *Remote Sensing*, 4(4), 950–974. https://doi.org/10.3390/rs4040950

Karan, M., Liddell, M., Prober, S. M., Arndt, S., Beringer, J., Boer, M., Cleverly, J., Eamus, D., Grace, P., van Gorsel, E., Hero, J.-M., Hutley, L., Macfarlane, C., Metcalfe, D., Meyer, W., Pendall, E., Sebastian,

A., & Wardlaw, T. (2016). The Australian SuperSite network: A continental, long-term terrestrial ecosystem observatory. *Science of the Total Environment*, *568*, 1263–1274. https://doi.org/10.1016/j.scitotenv.2016.05.170

Keränen, J., Maltamo, M., & Packalen, P. (2016). Effect of flying altitude, scanning angle and scanning mode on the accuracy of ALS based forest inventory. *International Journal of Applied Earth Observation and Geoinformation*, *52*, 349–360. https://doi.org/10.1016/j.jag.2016.07.005

Khosravipour, A., Skidmore, A. K., & Isenburg, M. (2016). Generating spike-free digital surface models using LiDAR raw point clouds: A new approach for forestry applications. *International Journal of Applied Earth Observation and Geoinformation*, *52*, 104–114. https://doi.org/10.1016/j.jag.2016.06.005

Khosravipour, A., Skidmore, A. K., Isenburg, M., Wang, T., & Hussin, Y. A. (2014). Generating pit-free canopy height models from airborne Lidar. *Photogrammetric Engineering & Remote Sensing*, *80*(9), 863–872. https://doi.org/10.14358/PERS.80.9.863

Koontz, M. J., North, M. P., Werner, C. M., Fick, S. E., & Latimer, A. M. (2020). Local forest structure variability increases resilience to wildfire in dry western U.S. coniferous forests. *Ecology Letters*, *23*(3), 483–494. https://doi.org/10.1111/ele.13447

Labriere, N., Tao, S., Chave, J., Scipal, K., le Toan, T., Abernethy, K., Alonso, A., Barbier, N., Bissiengou, P., Casal, T., Davies, S. J., Ferraz, A., Herault, B., Jaouen, G., Jeffery, K. J., Kenfack, D., Korte, L., Lewis, S. L., Malhi, Y., … Saatchi, S. (2018). In situ reference datasets from the TropiSAR and AfriSAR campaigns in support of upcoming Spaceborne biomass missions. *IEEE Journal of Selected Topics in Applied Earth Observations and Remote Sensing*, *11*(10), 3617–3627. https://doi.org/10.1109/JSTARS.2018.2851606

Lang, N., Jetz, W., Schindler, K., & Wegner, J. D. (2023). A high-resolution canopy height model of the Earth. *Nature Ecology & Evolution*, *7*(11), 1778–1789. https://doi.org/10.1038/s41559-023-02206-6

LaRue, E. A., Fahey, R., Fuson, T. L., Foster, J. R., Matthes, J. H., Krause, K., & Hardiman, B. S. (2022). Evaluating the sensitivity of forest structural diversity characterization to LiDAR point density. *Ecosphere*, *13*(9), e4209. https://doi.org/10.1002/ecs2.4209

Leitold, V., Keller, M., Morton, D. C., Cook, B. D., & Shimabukuro, Y. E. (2015). Airborne lidar-based estimates of tropical forest structure in complex terrain: Opportunities and trade-offs for REDD+. *Carbon Balance and Management*, *10*(1), 3. https://doi.org/10.1186/s13021-015-0013-x

Lines, E. R., Fischer, F. J., Owen, H. J. F., & Jucker, T. (2022). The shape of trees: Reimagining forest ecology in three dimensions with remote sensing. *Journal of Ecology*, *110*(8), 1730–1745. https://doi.org/10.1111/1365-2745.13944

Lobry, J. R., Bel-Venner, M.-C., Bogdziewicz, M., Hacket-Pain, A., & Venner, S. (2023). The CV is dead, long live the CV! *Methods in Ecology and Evolution*, *14*, 2780–2786. https://doi.org/10.1111/2041-210X.14197

Magnussen, S., Næsset, E., & Gobakken, T. (2010). Reliability of LiDAR derived predictors of forest inventory attributes: A case study with Norway spruce. *Remote Sensing of Environment*, *114*(4), 700–712. https://doi.org/10.1016/j.rse.2009.11.007

McNicol, I. M., Mitchard, E. T. A., Aquino, C., Burt, A., Carstairs, H., Dassi, C., Modinga Dikongo, A., & Disney, M. I. (2021). To what extent can UAV photogrammetry replicate UAV LiDAR to determine Forest structure? A test in two contrasting tropical forests. *Journal of Geophysical Research: Biogeosciences*, *126*(12), e2021JG006586. https://doi.org/10.1029/2021JG006586

Meer, P. J., & Bongers, F. (1996). Formation and closure of canopy gaps in the rain forest at Nouragues, French Guiana. *Vegetatio*, *126*(2), 167–179. https://doi.org/10.1007/BF00045602

Mielcarek, M., Stereńczak, K., & Khosravipour, A. (2018). Testing and evaluating different LiDAR-derived canopy height model generation methods for tree height estimation. *International Journal of Applied Earth Observation and Geoinformation*, *71*, 132–143. https://doi.org/10.1016/j.jag.2018.05.002

Morsdorf, F., Frey, O., Meier, E., Itten, K. I., & Allgöwer, B. (2008). Assessment of the influence of flying altitude and scan angle on biophysical vegetation products derived from airborne laser scanning. *International Journal of Remote Sensing*, *29*(5), 1387–1406. https://doi.org/10.1080/01431160701736349

Moudrý, V., Cord, A. F., Gábor, L., Laurin, G. V., Barták, V., Gdulová, K., Malavasi, M., Rocchini, D., Stereńczak, K., Prošek, J., Klápště, P., & Wild, J. (2023). Vegetation structure derived from airborne laser scanning to assess species distribution and habitat suitability: The way forward. *Diversity and Distributions*, *29*(1), 39–50. https://doi.org/10.1111/ddi.13644

Næsset, E. (2002). Predicting forest stand characteristics with airborne scanning laser using a practical two-stage procedure and field data. *Remote Sensing of Environment*, *80*(1), 88–99. https://doi.org/10.1016/S0034-4257(01)00290-5

Næsset, E. (2009). Effects of different sensors, flying altitudes, and pulse repetition frequencies on forest canopy metrics and biophysical stand properties derived from small-footprint airborne laser data. *Remote Sensing of Environment*, *113*(1), 148–159. https://doi.org/10.1016/j.rse.2008.09.001

Pearse, G. D., Watt, M. S., Dash, J. P., Stone, C., & Caccamo, G. (2019). Comparison of models describing forest inventory attributes using standard and voxel-based lidar predictors across a range of pulse densities. *International Journal of Applied Earth Observation and Geoinformation*, *78*, 341–351. https://doi.org/10.1016/j.jag.2018.10.008

Quan, Y., Li, M., Hao, Y., & Wang, B. (2021). Comparison and evaluation of different pit-filling methods for generating high resolution canopy height model using UAV laser scanning data. *Remote Sensing*, *13*(12), 2239. https://doi.org/10.3390/rs13122239

R Core Team. (2023). *R: A language and environment for statistical computing*. R Foundation for Statistical Computing. https://www.R-project.org/

Riofrío, J., White, J. C., Tompalski, P., Coops, N. C., & Wulder, M. A. (2022). Harmonizing multi-temporal airborne laser scanning point clouds to derive periodic annual height increments in temperate mixedwood forests. *Canadian Journal of Forest Research*, *52*(10), 1334–1352. https://doi.org/10.1139/cjfr-2022-0055

Rosen, A., Jörg Fischer, F., Coomes, D. A., Jackson, T. D., Asner, G. P., & Jucker, T. (2024). Tracking shifts in forest structural complexity through space and time in human-modified tropical landscapes. *Ecography*, e07377. https://doi.org/10.1111/ecog.07377

Roussel, J.-R., Auty, D., Coops, N. C., Tompalski, P., Goodbody, T. R. H., Meador, A. S., Bourdon, J.-F., de Boissieu, F., & Achim, A. (2020). lidR: An R package for analysis of Airborne Laser Scanning (ALS) data. *Remote Sensing of Environment*, *251*, 112061. https://doi.org/10.1016/j.rse.2020.112061

Roussel, J.-R., Béland, M., Caspersen, J., & Achim, A. (2018). A mathematical framework to describe the effect of beam incidence angle on metrics derived from airborne LiDAR: The case of forest canopies approaching turbid medium behaviour. *Remote Sensing of Environment*, *209*, 824–834. https://doi.org/10.1016/j.rse.2017.12.006

Roussel, J.-R., Caspersen, J., Béland, M., Thomas, S., & Achim, A. (2017). Removing bias from LiDAR-based estimates of canopy height: Accounting for the effects of pulse density and footprint size. *Remote Sensing of Environment*, *198*, 1–16. https://doi.org/10.1016/j.rse.2017.05.032

Silva, C. A., Valbuena, R., Pinagé, E. R., Mohan, M., de Almeida, D. R. A., North Broadbent, E., Jaafar, W. S. W. M., de Almeida Papa, D., Cardil, A., & Klauberg, C. (2019). ForestGapR: An r package for forest gap analysis from canopy height models. *Methods in Ecology and Evolution*, *10*(8), 1347–1356. https://doi.org/10.1111/2041-210X.13211

Tolan, J., Yang, H.-I., Nosarzewski, B., Couairon, G., Vo, H. V., Brandt, J., Spore, J., Majumdar, S., Haziza, D., Vamaraju, J., Moutakanni, T., Bojanowski, P., Johns, T., White, B., Tiecke, T., & Couprie, C. (2024). Very high resolution canopy height maps from RGB imagery using self-supervised vision transformer and convolutional decoder trained on aerial lidar. *Remote Sensing of Environment*, *300*, 113888. https://doi.org/10.1016/j.rse.2023.113888

Tompalski, P., White, J. C., Coops, N. C., & Wulder, M. A. (2019). Demonstrating the transferability of forest inventory attribute models derived using airborne laser scanning data. *Remote Sensing of Environment*, *227*, 110–124. https://doi.org/10.1016/j.rse.2019.04.006

Vincent, G., Verley, P., Brede, B., Delaitre, G., Maurent, E., Ball, J., Clocher, I., & Barbier, N. (2023). Multi-sensor airborne lidar requires inter-calibration for consistent estimation of light attenuation and plant area density. *Remote Sensing of Environment*, *286*, 113442. https://doi.org/10.1016/j.rse.2022.113442

Wagner, F. H., Roberts, S., Ritz, A. L., Carter, G., Dalagnol, R., Favrichon, S., Hirye, M. C. M., Brandt, M., Ciais, P., & Saatchi, S. (2024). Sub-meter tree height mapping of California using aerial images and LiDAR-informed U-Net model. *Remote Sensing of Environment*, *305*, 114099. https://doi.org/10.1016/j.rse.2024.114099

Wedeux, B. M. M., & Coomes, D. A. (2015). Landscape-scale changes in forest canopy structure across a partially logged tropical peat swamp. *Biogeosciences*, *12*(22), 6707–6719. https://doi.org/10.5194/bg-12-6707-2015

Wilkes, P., Jones, S. D., Suarez, L., Haywood, A., Woodgate, W., Soto-Berelov, M., Mellor, A., & Skidmore, A. K. (2015). Understanding the effects of ALS pulse density for metric retrieval across diverse forest types. *Photogrammetric Engineering & Remote Sensing*, *81*(8), 625–635. https://doi.org/10.14358/PERS.81.8.625

Zellweger, F., Braunisch, V., Baltensweiler, A., & Bollmann, K. (2013). Remotely sensed forest structural complexity predicts multi species occurrence at the landscape scale. *Forest Ecology and Management*, *307*, 303–312. https://doi.org/10.1016/j.foreco.2013.07.023

Zhang, B., Fischer, F. J., Coomes, D. A., & Jucker, T. (2023). Logging leaves a fingerprint on the number, size, spatial configuration and geometry of tropical forest canopy gaps. *Biotropica*, *55*(2), 354–367. https://doi.org/10.1111/btp.13190

Zhang, B., Fischer, F. J., Prober, S. M., Yeoh, P. B., Gosper, C. R., Zdunic, K., & Jucker, T. (2024). Robust retrieval of forest canopy structural attributes using multi-platform airborne LiDAR. *Remote Sensing in Ecology and Conservation*. https://doi.org/10.1002/rse2.398

SUPPORTING INFORMATION

Additional supporting information can be found online in the Supporting Information section at the end of this article.

Appendix A: Supplementary text.

Appendix B: Tables.

Appendix C: Figures.

Appendix D: Replication study.

Appendix E: Literature.

How to cite this article: Fischer, F. J., Jackson, T., Vincent, G., & Jucker, T. (2024). Robust characterisation of forest structure from airborne laser scanning—A systematic assessment and sample workflow for ecologists. *Methods in Ecology and Evolution*, *15*, 1873–1888. https://doi.org/10.1111/2041-210X.14416